Rate coefficients of the H + H_2O_2 → H_2 + HO_2 reaction on an accurate fundamental invariant-neural network potential energy surface

Xiaoxiao Lu, Qingyong Meng, Xingan Wang, Bina Fu, and Dong H. Zhang

Citation: J. Chem. Phys. **149**, 174303 (2018); doi: 10.1063/1.5063613
View online: https://doi.org/10.1063/1.5063613
View Table of Contents: http://aip.scitation.org/toc/jcp/149/17
Published by the American Institute of Physics

Rate coefficients of the H + H_2O_2 → H_2 + HO_2 reaction on an accurate fundamental invariant-neural network potential energy surface

Xiaoxiao Lu,[1,2] Qingyong Meng,[3] Xingan Wang,[1] Bina Fu,[2,a)] and Dong H. Zhang[2,b)]
[1]*Department of Chemical Physics, University of Science and Technology of China, Jinzhai Road 96, Hefei 230026, China*
[2]*State Key Laboratory of Molecular Reaction Dynamics and Center for Theoretical and Computational Chemistry, Dalian Institute of Chemical Physics, Chinese Academy of Sciences, Zhongshan Road 457, Dalian 116023, China*
[3]*Department of Applied Chemistry, Northwestern Polytechnical University, Youyi West Road 127, Xi'an 710072, China*

(Received 28 September 2018; accepted 18 October 2018; published online 2 November 2018)

The rate coefficients of the H + H_2O_2 → H_2 + HO_2 reaction are calculated using the ring polymer molecular dynamics (RPMD), quasi-classical trajectory (QCT), and canonical variational transition state theory (CVT) with small curvature tunneling (SCT) correction, in conjunction with the recently constructed fundamental invariant-neural network (FI-NN) potential energy surface (PES) [X. Lu *et al.*, Phys. Chem. Chem. Phys. **20**, 23095 (2018)]. In RPMD calculations, 32, 16, and 8 beads are used for computing the rate coefficients at 200 K ≤ T ≤ 400 K, 500 K ≤ T ≤ 700 K, and 700 K < T ≤ 1000 K, respectively. Given that the previous experimental rate coefficients vary widely, in particular, at low temperatures, the present RPMD rate coefficients agree well with most of the experimental results. In addition, comparing with some experimental values, the present QCT and CVT/SCT calculations on the FI-NN PES also predict accurate results at some temperatures. These results strongly support the accuracy of the present dynamics calculations as well as the full-dimensional FI-NN PES. *Published by AIP Publishing.* https://doi.org/10.1063/1.5063613

I. INTRODUCTION

It is well-known that accurate rate coefficients of various elementary reactions in the combustion system are prerequisite, to deeply understand the combustion and explosion processes of fuels. Over the past decades, the H_2/O_2 combustion system was theoretically and experimentally investigated over a rather large temperature range.[1–15] All of these studies proposed that, because it produces a very important clean energy source H_2 and a radical-chain breaking species HO_2,[6,16,17] the H + H_2O_2 → H_2 + HO_2 reaction plays a critical role in fundamental combustion chemistry of H_2/O_2. Thus, its rate coefficients are very important for kinetic studies on H_2/O_2 combustion.

Experimentally, the rate coefficients of H + H_2O_2 → H_2 + HO_2 were measured by several laboratories,[2,3,5,6,9,10,12] in particular, at room temperature.[2,6,9,12] Unexpectedly, these experimental values differ from each other by almost two orders of magnitude. Theoretically, Truhlar and co-workers[1] computed the rate coefficients of the title reaction using canonical variational transition state theory (CVT) with multidimensional tunneling.[18,19] In their work, the M05-2X/MG3S functional was employed to determine the barrier height of the title reaction and the CVT rate coefficients fall between the experimental results.[3,5,9] Moreover, a variational transition state theory (VTST) with interpolated single-point energy calculation for best estimating the barrier height was also employed. Although their calculations[18,19] predicted the rate coefficients being in good agreement with the experimental results,[3,5] artificial estimation of the barrier height is still needed making the whole calculations be not *ab initio*. In this work, we accurately computed the rate coefficients of the title reaction based on an accurate full-dimensional potential energy surface (PES) by fundamental invariant-neural network (FI-NN) fitting to extensive energy points, which were calculated by the unrestricted coupled-cluster singles, doubles, and perturbative triples (UCCSD(T)) method with the aug-cc-pVTZ basis.[20]

From the viewpoint of theory, in order to accurately compute rate coefficients, full-dimensional quantum dynamics together with extensive quantum statistical-mechanical samplings are needed. From the viewpoint of calculation, however, there still exists a big challenge in computing rate coefficients at low temperatures. For example, although a modern wave packet propagation algorithm is very accurate for small systems,[21–27] it fails in larger systems due to its quite huge computational cost. In the past two decades, tremendous efforts have been devoted to developing approximate methods to incorporate important quantum effects in calculating rate coefficients for larger systems.[28–35] One of the examples is the ring-polymer molecular dynamics (RPMD) method,[31–35] which makes good use of the isomorphism between a quantum mechanical system and a fictitious classical ring polymer. This ring polymer consists of many replications of the original system connected by harmonic springs which are called

[a)]Electronic mail: bina@dicp.ac.cn
[b)]Electronic mail: zhangdh@dicp.ac.cn

as beads. The evolution of RPMD is accomplished by Newtonian dynamics, but it gives nearly the exact quantum statistics, which considers important quantum effects such as the tunneling and zero-point energy. Many recent studies on the polyatomic reactions[36–53] demonstrated that the RPMD is capable of giving fairly accurate rates even at low temperatures in the deep tunneling regime with a sufficient number of beads.

In order to accurately compute the rate coefficients of the title reaction, the RPMD calculations are performed in this work. For comparison, quasi-classical trajectory (QCT) calculations and CVT with small curvature tunneling (SCT) corrections are also performed in this work. Obviously, a PES is prerequisite in performing dynamics calculations. Recently, a new global full-dimensional PES of the $H + H_2O_2$ system was constructed[20] by the fundamental invariant neural-network (FI-NN) fitting method.[54] The small fitting error (5.7 meV)[20] of this PES establishes the foundation of the present work.

This paper is organized as follows. Section II gives computational details of this work. In Sec. III, we present numerical details, results, and discussions. Finally, Sec. IV concludes with a summary.

II. COMPUTATIONAL DETAILS

A. Computational approaches

In this work, all RPMD calculations are carried out using the RPMDrate code.[55] Since details of RPMD have been well reviewed elsewhere,[32–34,36,56–58] only brief notes are given here. Setting $\mathbf{p} = \{\mathbf{p}_i\}_{i=1}^N$, $\mathbf{r} = \{\mathbf{r}_i\}_{i=1}^N$, and m_i be momenta, positions, and mass of the ith atom, respectively, the RPMD Hamiltonian[31–34] was proved in the form

$$H_n(\mathbf{p},\mathbf{r}) = \sum_{j=1}^{n}\left[\sum_{i=1}^{N}\left(\frac{\left|\mathbf{p}_i^{(j)}\right|^2}{2m_i} + \frac{1}{2}m_i\omega_n^2\left|\mathbf{r}_i^{(j)} - \mathbf{r}_i^{(j-1)}\right|^2\right) + V\left(\mathbf{r}_1^{(j)},\ldots,\mathbf{r}_N^{(j)}\right)\right], \quad \mathbf{r}_i^{(0)} \equiv \mathbf{r}_i^{(n)}, \tag{1}$$

where $\omega_n = nk_BT/\hbar$ is the force constant between two neighboring beads, $V(\mathbf{r}_1,\ldots,\mathbf{r}_N)$ is the PES of the system. In Eq. (1), $\mathbf{p}_i^{(j)}$ and $\mathbf{r}_i^{(j)}$ are the momentum and Cartesian coordinate of the jth bead of the ith atom, respectively, where the superscript j means the quantity of the jth bead. Turning to the RPMD rate coefficient,[33,34,36,55] the Bennett-Chandler factorization[59,60] gives the form

$$k_{\mathrm{RPMD}}^{(n)}(T) = \kappa^{(n)}\left(t\to\infty, T, \xi^{\ddagger}\right)\cdot\exp\left(-\frac{\Delta W^{(n)}(T)}{k_BT}\right)\cdot 4\pi R_\infty^2\left(\frac{k_BT}{2\pi\mu}\right)^{\frac{1}{2}}, \tag{2}$$

where $\kappa^{(n)}(t\to\infty, T, \xi^{\ddagger})$ is the long-time limit of a time-dependent ring-polymer transmission coefficient, which accounts for the recrossing at the peak position $\xi^{\ddagger}$ of the free-energy curve along the reaction coordinate $\xi(\mathbf{r})$. The transmission coefficient reaches a plateau value relatively quickly at t_p, which is the "plateau" time, and no long-time propagation is needed. Therefore, $\kappa^{(n)}(t\to\infty, T, \xi^{\ddagger}) \simeq \kappa^{(n)}\left(t_p, T, \xi^{\ddagger}\right)$.

In the second term of Eq. (2), $\Delta W^{(n)}(T)$ is the free-energy barrier, which can be computed by umbrella integration.[61–63] In the third term of Eq. (2), μ is the reduced mass between the two reactants and R_∞ is a parameter that is sufficiently large as to make the interaction between the reactants negligible.

In this work, the QCT and CVT/SCT calculations are also performed to compute the rate coefficient. The QCT rate coefficient[64] computed on the FI-NN PES[20] of the single electronic state is given in the form

$$k_{\mathrm{QCT}}(T) = \pi b_{\max}^2\sqrt{\frac{8k_BT}{\pi\mu}}\frac{N_r}{N_{\mathrm{total}}}, \tag{3}$$

where $b_{\max}$ is the maximum impact parameter. In addition, the parameters N_r and N_{total} are numbers of the reactive and total trajectories, respectively. In QCT calculations, initial conditions including the translational, vibrational, and rotational states for reactants are chosen by sampling a Boltzmann distribution at a given temperature.

For comparing with the above trajectory-based calculations, the CVT/SCT calculations are performed using the POLYRATE procedure,[65] while all geometries of reactants, products, and transition state (TS) used for CVT/SCT are optimized from the FI-NN PES.[20] In this method, the tunneling is approximated by using the small curvature tunneling correction, which is smaller than the microcanonical optimized multidimensional tunneling (μOMT) approach. We refer the readers to Refs. 19, 65, and 66 for the technical details.

B. Numerical details

In this work, all the calculated rate coefficients of the $H + H_2O_2 \to H_2 + HO_2$ reaction are based on the FI-NN PES,[20] which was fitted to a 26-50-60-1 NN-structure function with 4471 parameters, using ~110 000 UCCSD(T)/aug-cc-pVTZ energy points. The training and validating deviations of the FI-NN PES are 5.3 and 8.4 meV, respectively, which lay solid foundations for dynamics calculations. We show the numerical details of the present dynamics calculations below.

First, the input parameters used in the present RPMD calculations are summarized in Table I. In computing the free-energy barrier, the reaction coordinate is divided into 110 windows with the same interval. Two sets of the force constant of the biasing potential of k were used. In the asymptotic region ($\xi \in [-0.05, 0.90]$), $k = k_0 = 2.727(T/\mathrm{K})$ eV was used at all temperatures and k_0 was always used at low temperatures for each sampling window. While in the region near the barrier ($\xi \in [0.91, 1.05]$), larger force constant k values ($2k_0$–$3k_0$) were used at higher temperatures ($T \geq 500$ K) accordingly. In each sampling window, the system was equilibrated for 10 ps initially, following by a production evolution of 50 ps. The time step here is set to 0.1 fs. The Andersen thermostat was used in all simulations with a default 100 fs sampling time.

After the free-energy calculations, the transmission coefficients were calculated accordingly. Specifically, after having acquired the optimal value of the reaction coordinate from the potential of mean force, a series of configurations at the transition state dividing surface were generated on the

TABLE I. Input parameters for the RPMD rate calculations for the $H + H_2O_2 \rightarrow H_2 + HO_2$ reaction.

Parameter		$H + H_2O_2 \rightarrow H_2 + HO_2$		Explanation
Command line parameters				
Temp	200	500	1000	Temperature (K)
	298	700		
	400			
N_{beads}	32	16	8	Number of beads
Dividing surface parameters				
R_∞		16		Dividing surface s1 parameter (a_0)
N_{bond}		1		Number of forming and breaking bonds
N_{channel}		2		Number of equivalent product channels
Thermostat		"Andersen"		Thermostat option
Biased sampling parameters				
N_{windows}		111		Number of windows
ξ_1		–0.05		Center of the first window
$d\xi$		0.01		Window spacing step
ξ_N		1.05		Center of the last window
dt		0.0001		Time step (ps)
K_i		2.72		Umbrella force constant ((T/K) eV)
		5.44 ($\xi \in [0.91, 1.05]$, $T = 700$ K)		
		8.16 ($\xi \in [0.91, 1.05]$, $T = 1000$ K)		
$M_{\text{trajectory}}$		100		Number of trajectories
$t_{\text{equilibration}}$		10		Equilibration period (ps)
t_{sampling}		50		Sampling period in each trajectory (ps)
N_{i}		5×10^7		Total number of sampling points
Potential of mean force calculation				
ξ_0		–0.02		Start of umbrella integration
ξ_t		1.05		End of umbrella integration
N_{bins}		5000		Number of bins
Recrossing factor calculation				
dt		0.0001		Time step (ps)
$t_{\text{equilibration}}$		20		Equilibration period (ps) in the constrained (parent) trajectory
$N_{\text{totalchild}}$		100 000		Total number of unconstrained (child) trajectories
$t_{\text{childsampling}}$		2		Sampling increment along the parent trajectory (ps)
N_{child}		100		Number of child trajectories per one initially constrained configuration
t_{child}		0.05		Length of child trajectories (ps)

accurate FI-NN PES. For each of these constrained configurations, a parent trajectory with the ring-polymer centroid fixed at the top of the free-energy barrier was equilibrated for 20 ps with a time step of 0.1 fs using the RATTLE algorithm.[67] Configurations were sampled once every 2 ps to serve as the initial positions for the child trajectories, which were used in calculating the flux-side correlation function. A set of 100 child trajectories were spawned with different initial momenta sampled from a Maxwell-Boltzmann distribution. These trajectories were propagated with no constraint/thermostat for 0.05 ps where the transmission coefficients reach plateau values. A total of 100 000 child trajectories were propagated to obtain the converged $\kappa^{(n)}$ at a given temperature.

Turning to the QCT calculations, the initial distance of the H atom from the center of mass of H_2O_2 was $\sqrt{x^2 + b^2}$, where b is the impact parameter and x was set to 11.0 bohrs. The trajectories were terminated when the distance of two fragments became larger than 13.0 bohrs. The evolution of QCT trajectories was performed using the Velocity-Verlet integration algorithm with a time step of 0.073 fs for a maximum time of 50 ps. The maximum impact parameter (b_{max}) was set to different values at different temperatures after many tests. For example, we set $b_{\text{max}} = 8.5$ bohrs at $T = 300$ and 400 K after extensive thermal QCT calculations because of the extremely small reaction probabilities. (At 300 K, only $2H + H_2O_2$ reactive trajectories occur in 1.0×10^6 trajectories.) The reaction probabilities naturally become larger as the temperature rises. The b_{max} is 8.7, 9.2, and 9.6 bohrs at 500 K, 700 K, and 900 K, respectively. The b_{max} even rises to 10 bohrs with a relatively large reaction probability ($N_r/N_{\text{total}} = 0.04\%$) at 1000 K. Roughly 1.0×10^9 and 1.0×10^6 trajectories were calculated at low and high temperatures, respectively. The number of trajectories we run is huge, resulting in an overall convergence error of less than 1%.

III. RESULTS AND DISCUSSIONS

A. Convergence inspections of RPMD

The free-energy curves with different numbers of beads at 200 K and 400 K are displayed in Figs. 1(a) and 1(b), respectively. Apparently, pure classical $\Delta W^{(n=1,T)}$ at these two temperatures are significantly higher than those obtained with more beads, suggesting that the reaction is significantly influenced by tunneling and zero-point energy. It is reasonable to suppose that quantum-statistical effects on the free energy barrier are remarkable. At 200 K, $\Delta W^{(n=8)}$ is much smaller than the others $\Delta W^{(n\geq 16)}$ by 14 meV, which indicates that setting n = 8 is far from enough to make the free-energy barrier converged. Therefore, a larger number of beads were applied to perform RPMD simulations for $\Delta W^{(n)}$. As we expected, the difference between the free energy barriers becomes smaller as the number of beads increases. The difference between $\Delta W^{(n=16)}$ and $\Delta W^{(n=32)}$ is 1.6 meV, while the difference between $\Delta W^{(n=32)}$ and $\Delta W^{(n=64)}$ is fairly small, indicating 32 beads are sufficient to converge the free-energy barrier at 200 K. According to the performance of $\Delta W^{(n)}$ at 200 K, the same strategy was used to check the convergence of free-energy barriers at 400 K. The difference between $\Delta W^{(n=16)}$ and $\Delta W^{(n=32)}$ is 1.4 meV at 400 K, which will introduce less than 7% errors to $\exp(-\beta\Delta W)$. Based on this fact, 16 beads are adequate to make the free-energy barrier converged for the title reaction on the current PES. In order to obtain more accurate results, we set n = 32 at low temperatures such as 200 K, 298 K, and 400 K, where there are significant quantum-statistical effects on the free-energy barriers. Also, 16 beads were employed to perform RPMD simulations at medium temperatures such as 500 K and 700 K, while 8 beads are enough for 1000 K after inspection. It is interesting that the free energy barrier height is not a monotonically decreasing function of the number of beads. The same behavior was also seen previously in the RPMD calculations for the HCl + OH → Cl + H_2O reaction.[50] However, it is still an open question on the relationship between the free-energy barrier and the number of beads.

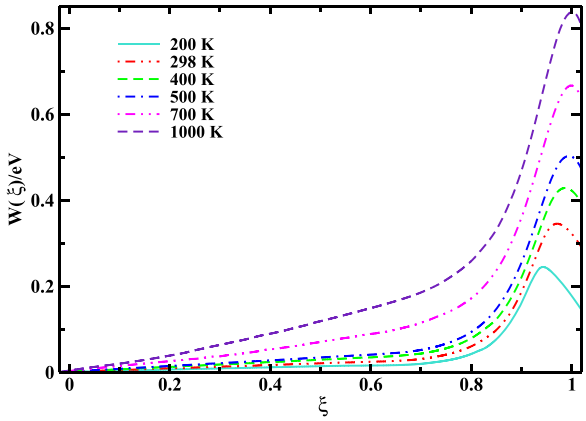

FIG. 2. Temperature dependence of the free-energy curves for the H + H_2O_2 → H_2 + HO_2 reaction.

The converged RPMD free-energy curves at 200 K ≤ T ≤ 1000 K are shown in Fig. 2. We can see that the positions of all free-energy barriers (ξ) are getting closer to 1.0 as the reaction temperature rises, indicating that the title reaction is activated near the PES barrier. Reasonably, the whole free-energy curve is monotonically increasing as the temperature rises as well as the free-energy barrier. For instance, the ΔW is 0.34 eV at room temperature but 0.66 eV at 700 K. The free-energy barrier increases from 0.24 eV at 200 K to 0.83 eV at 1000 K with a range of 0.6 eV.

Similar to the convergence inspections for free-energy, as shown in Figs. 3(a) and 3(b), with respect to the number

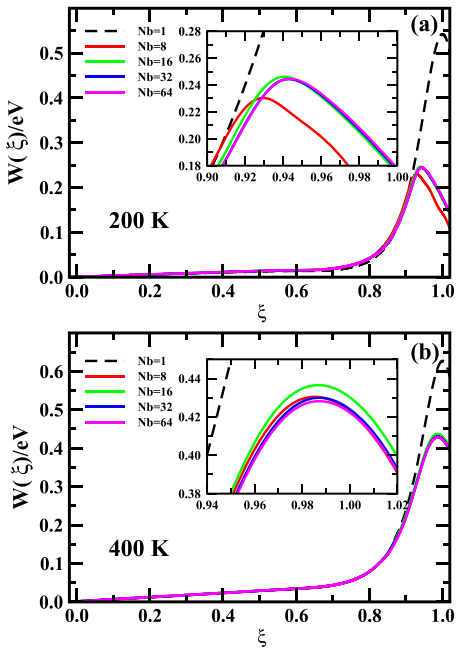

FIG. 1. (a) Comparison of the free-energy curves with different bead numbers for the H + H_2O_2 → H_2 + HO_2 reaction at 200 K. (b) The same as (a), except at 400 K.

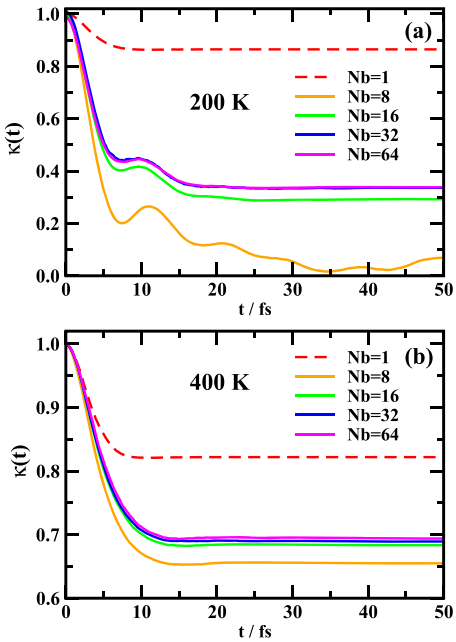

FIG. 3. (a) Comparison of the transmission coefficients with different bead numbers for the H + H_2O_2 → H_2 + HO_2 reaction at 200 K. (b) The same as (a), except at 400 K.

of polymer beads, we set n = 1, 8, 16, 32, 64 to check the convergence of $\kappa^{(n)}$. It seems obvious that all the transmission coefficient values decay quickly within 8 fs and reach plateau within no more than 20 fs. In particular, the transmission coefficient curve at 200 K shows a small oscillation during 8–15 fs, much more likely caused by quantum effects during the transfer of the H atom at low temperatures. Such an oscillation does not appear in the transmission coefficient curves at 400 K. From Fig. 3, we can see that a set of smooth transmission coefficient curves with different numbers of polymer beads quickly reach plateau after a short time decay. It is obvious that the classical recrossing factor with a single bead at these two temperatures is closed to 1.0, which is significantly higher than the RPMD recrossing factor ($n \geq 8$). At 200 K, $\kappa^{(n=1)}$ is about 1.6 times $\kappa^{(n\geq 8)}$, while 1.2 times at 400 K. Such remarkable differences between classical and RPMD transmission coefficients imply that the quantum effects of the reaction system can strongly influence the rate coefficient.

The convergence of transmission coefficients using different beads at a given temperature is discussed below. For instance, at 200 K, $\kappa^{(n\geq 8)}$ gradually increases as the number of beads increases and becomes converged eventually. The resulting $\kappa^{(n=8)}$ and $\kappa^{(n=16)}$ are smaller than $\kappa^{(n=32)}$ by 12% and 10%, respectively, while $\kappa^{(n=64)}$ is bigger than $\kappa^{(n=32)}$ by smaller than 1%. According to the performance of the above set of transmission coefficient curves, the $\kappa^{(n)}$ values are easily influenced by the number of ring polymer beads at low temperatures and $\kappa^{(n)}$ is converged until the value of n increases to 32. As the given temperature rises, $\kappa^{(n)}$ converges more quickly. For example, $\kappa^{(n=16)}$ obviously has converged with a slight 1% difference compared with $\kappa^{(n=32)}$ at 400 K. Based on the above convergence inspections, 32, 16, and 8 polymer beads were used to compute $\kappa^{(n)}$ at T < 500 K, 500 K ≤ T ≤ 700 K, and T > 700 K, respectively.

The RPMD transmission coefficients κ as a function of time at various temperatures are shown in Fig. 4. Obviously, all the transmission coefficient values decay quickly within 8 fs and reach plateau within 20 fs. Only the transmission coefficient curve at 200 K shows small oscillation structures during 8–15 fs, which arise from the transfer of the H atom in the deep quantum tunneling regime. Note that the calculated crossover temperature is roughly 544 K for this reaction. The transmission coefficients are monotonically increasing as temperature rises as the same way as the free-energy curves in Fig. 2. The $\kappa(t)$ increases from 0.338 at 200 K to 0.778 at 1000 K. In particular, the growth rate is slowing down. We can see that the transmission coefficient at 1000 K is only 0.008 larger than that at 700 K.

B. Rate coefficients

Here, we report rate coefficients at temperatures between 200 K and 1000 K in an Arrhenius plot, as shown in Fig. 5. The numerical results of the present $k^{(n)}_{\mathrm{RPMD}}(T)$, k_{QCT}, and $k_{\mathrm{CVT/SCT}}$ values, together with the available experimental rate coefficients, are given in Table II.

From Fig. 5, one can find that the calculated RPMD results (red solid line with square symbols) are in good agreement with most of the experimental values. At high temperatures, the rate coefficients k_{RPMD} (700 K ≤ T ≤ 1000 K) have given a good estimate with respect to the experimental values (the three left triangles with maroon color) from Baldwin and co-workers in 1970. The maximum difference between the RPMD line and that measured by Baldwin and co-workers in 1979 (the single orange right triangle) is ~25%, which may be caused by the less accuracy of $\Delta W(T)$. While in this temperature range, rate coefficients obtained from QCT calculations (the green dashed line with up triangles) are generally larger than those of RPMD and CVT/SCT (the violet dashed line with diamonds). Particularly the QCT calculations yield a rate of 4.15×10^{-13} cm^3 molecule^{-1} s^{-1} at 773 K, well matched with the experimental value (4.32×10^{-13} cm^3 molecule^{-1} s^{-1}) from Baldwin and co-workers. The rate coefficients from QCT calculations can give a fairly good estimate at high temperatures, where the quantum effects are insignificant. At 300 K ≤ T ≤ 700 K, the slope of the Arrhenius plot of RPMD falls between that of CVT/SCT and QCT.

As shown in Fig. 5, several experimental values (black diamonds) from Albers and co-workers are coincident with the CVT/SCT and RPMD results. For example, an experimental rate coefficient of 1.57×10^{-14} cm^3 molecule^{-1} s^{-1} at 360 K is between the RPMD results (1.16×10^{-14} cm^3 molecule^{-1} s^{-1}) and the CVT/SCT results (1.83×10^{-14} cm^3 molecule^{-1} s^{-1}) with small differences by 28% and 16%, respectively. As a result, the performance of the variational

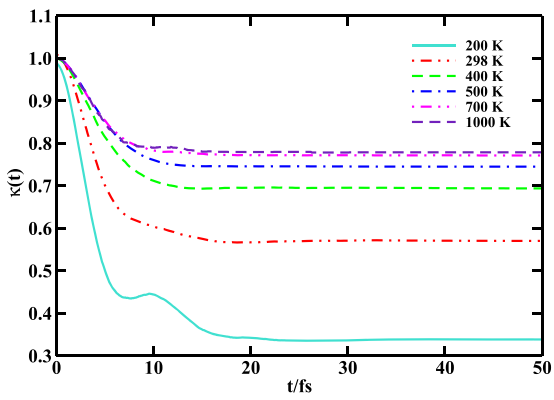

FIG. 4. Time dependence of the transmission coefficients for the H + H_2O_2 → H_2 + HO_2 reaction.

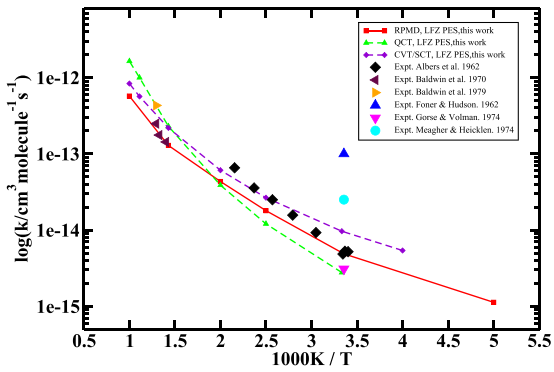

FIG. 5. Comparison of rate coefficients (in cm^3 molecule^{-1} s^{-1}) for the H + H_2O_2 → H_2 + HO_2 reaction obtained from the RPMD (this work), QCT (this work), and CVT/SCT (this work) approaches, together with the available experimental data recommended by Ref. 68.

TABLE II. Summary of the rate coefficients (in cm^3 $molecule^{-1}$ s^{-1}) for the $H + H_2O_2 \rightarrow H_2 + HO_2$ reaction obtained by the RPMD, QCT, and CVT/SCT methods, together with the available experimental values recommended by Ref. 68.

	Rate coefficient			
T/K	RPMD	QCT	CVT/SCT	Expt.
200	1.13×10^{-15} (32)		5.40×10^{-15} (250 K)	
				5.21×10^{-15} (294 K)
				5.28×10^{-15} (297 K)
298	4.89×10^{-15} (32)	2.77×10^{-15}	9.67×10^{-15}	3.1×10^{-15}
				2.51×10^{-14}
				1.0×10^{-13}
				4.86×10^{-15} (299 K)
				9.28×10^{-15} (328 K)
				1.57×10^{-14} (358 K)
400	1.80×10^{-14} (32)	1.21×10^{-14}	2.66×10^{-14}	2.50×10^{-14} (389 K)
				3.57×10^{-14} (422 K)
500	4.34×10^{-14} (16)	3.88×10^{-14}	6.10×10^{-14}	6.57×10^{-14} (464 K)
700	1.29×10^{-13} (16)	2.30×10^{-13}	2.19×10^{-13}	1.43×10^{-13} (713 K)
				1.76×10^{-13} (753 K)
				2.49×10^{-13} (773 K)
				4.32×10^{-13} (773 K)
900		9.99×10^{-13}	5.66×10^{-13}	
1000	5.72×10^{-13} (8)	1.64×10^{-12}	8.36×10^{-13}	

transition-state theory with an approximated small-curvature tunneling in computing the rate coefficients of the $H + H_2O_2 \rightarrow H_2 + HO_2$ reaction at medium temperatures is not so poor as other reactions.[19,66] However, the CVT/SCT approach overestimates the rate coefficients at low temperatures. We can find that a rate of 9.67×10^{-15} cm^3 $molecule^{-1}$ s^{-1} computed by CVT/SCT at 298 K is obviously larger than the experimental data (5.28×10^{-15} cm^3 $molecule^{-1}$ s^{-1}) by an error of ~83%. It is supposed that the CVT/SCT treatment of deep tunneling might not entirely be suitable here. Not as good as the RPMD results at medium temperatures, the underestimation by the QCT approach can be found compared with the experimental data. For instance, the QCT result at 400 K is ~0.43 times smaller than the experimental data given by Albers because the QCT calculations cannot describe well the quantum zero point energy and tunneling effects. At 298 K, larger differences can be found between the rate coefficients from QCT calculations and from Albers and co-workers. Interestingly, the QCT rate shows a good agreement compared with the experimental value measured by Gorse and Volman in 1974. By contrast, the rate coefficients calculated by the RPMD approach are in good agreement with the data from Albers, particularly, at 298 K. Although there is no available experimental values at 200 K, the rate coefficients of RPMD are reliable throughout the temperature range.

IV. CONCLUSIONS

To summarize, we employed three theoretical methods including ring polymer molecular dynamics (RPMD), quasi-classical trajectory (QCT), and CVT/SCT (CVT with the small curvature tunneling correction) to compute the rate coefficients of the $H + H_2O_2 \rightarrow H_2 + HO_2$ reaction on the recently reported FI-NN PES.[20] It is shown that this reaction is strongly influenced by the quantum mechanical tunneling and recrossing, particularly, at low temperatures. For the RPMD calculations, different numbers of beads are used in computing free-energy barrier $\Delta W^{(n)}(T)$ and transmission coefficient $k^{(n)}_{\mathrm{RPMD}}(T)$ by convergence inspection. Since the previous experimental rate coefficients vary widely, particularly, at low temperatures, the current RPMD rate coefficients agree well with most of the experimental results. Most of the relative differences between $k^{(n)}_{\mathrm{RPMD}}(T)$ and $k_{\mathrm{expt.}}(T)$ are smaller than 20%. Particularly at 700 K and room temperature, the RPMD results are almost as same as those of Baldwin and Albers.

In addition, extensive quasi-classical trajectory (QCT) calculations of the title reaction were also performed to obtain the rate coefficients at various temperatures. It was found that the QCT thermal rate coefficients are in reasonably good agreement with the experimental data at high temperatures. At 300 K $\leq T \leq$ 500 K, the QCT thermal rates are substantially underestimated, due to the strong quantum tunneling effects at low temperatures. Interestingly, a slight difference between QCT result (2.78×10^{-15} cm^3 $molecule^{-1}$ s^{-1}) and that of Gorse [$(3.1 \pm 0.8) \times 10^{-15}$ cm^3 $molecule^{-1}$ s^{-1}] at 298 K presents an excellent agreement. Similarly, the CVT/SCT rate coefficients are also in good agreement with experimental values at $T \geq$ 400 K. While at $T \leq$ 300 K, the CVT/SCT result shows about 50% overestimation by comparing with experimental values from Albers and Gorse.

ACKNOWLEDGMENTS

Bina Fu thanks Xueming Yang and Rex T. Skodje for many useful discussions on this reactive system. This work was

supported by the National Key R&D Program of China (Grant No. 2016YFF0200500), the National Natural Science Foundation of China (Grant Nos. 21722307, 21673233, 21503214, 21773186, 21433009, and 21688102), the Strategic Priority Research Program of the Chinese Academy of Sciences (Grant No. XDB17000000), and Hundred-Talent Program of Shaanxi.

[1]B. A. Ellingson, D. P. Theis, O. Tishchenko, J. Zheng, and D. G. Truhlar, J. Phys. Chem. A **111**, 13554 (2007).
[2]E. A. Albers, K. Hoyermann, H. G. Wagner, and J. Wolfrum, Symp. Combust. **13**, 81 (1971).
[3]R. R. Baldwin, D. Brattan, B. Tunnicliffe, R. W. Walker, and S. J. Webster, Combust. Flame **15**, 133 (1970).
[4]R. R. Baldwin, D. Jackson, R. W. Walker, and S. J. Webster, Trans. Faraday Soc. **63**, 1676 (1967).
[5]R. R. Baldwin and R. W. Walker, J. Chem. Soc., Faraday Trans. 1 **75**, 140 (1979).
[6]S. N. Foner and R. L. Hudson, J. Chem. Phys. **36**, 2681 (1962).
[7]W. Forst and P. A. Giguere, J. Phys. Chem. **62**, 340 (1958).
[8]R. A. Gorse and D. H. Volman, J. Photochem. **1**, 1 (1972).
[9]R. A. Gorse and D. H. Volman, J. Photochem. **3**, 115 (1974).
[10]H. Kijewski and J. Troe, Int. J. Chem. Kinet. **3**, 223 (1971).
[11]R. B. Klemm, W. A. Payne, and L. J. Stief, in *1st Symposium Chemical Kinetics Data for the Upper and Lower Atmosphere* (Wiley-Interscience, New York, 1975), pp. 61–72.
[12]J. F. Meagher and J. Heicklen, J. Photochem. **3**, 455 (1974).
[13]J. V. Michael, D. A. Whytock, J. H. Lee, W. A. Payne, and L. J. Stief, J. Chem. Phys. **67**, 3533 (1977).
[14]W. Tsang and R. F. Hampson, J. Phys. Chem. Ref. Data **15**, 1087 (1986).
[15]J. Warnatz, in *Combustion Chemistry*, edited by W. C. Gardiner (Springer US, New York, NY, 1984), pp. 197–360.
[16]B. Lewis and G. von Elbe, *Combustion, Flames and Explosions of Gases*, 2nd ed. (Academic Press, New York, 1961).
[17]W. C. Schumb, C. N. Satterfield, and R. L. Wentworth, *Hydrogen Peroxide* (Reinhold Publishing Corporation, New York, 1955).
[18]D. G. Truhlar and B. C. Garrett, Acc. Chem. Res. **13**, 440 (1980).
[19]V. S. Melissas and D. G. Truhlar, J. Chem. Phys. **99**, 3542 (1993).
[20]X. Lu, K. Shao, B. Fu, X. Wang, and D. H. Zhang, Phys. Chem. Chem. Phys. **20**, 23095 (2018).
[21]H. Song and H. Guo, J. Phys. Chem. A **119**, 826 (2015).
[22]B. Fu and D. H. Zhang, J. Chem. Phys. **138**, 184308 (2013).
[23]Y. Zhou and D. H. Zhang, J. Chem. Phys. **141**, 194307 (2014).
[24]B. Fu and D. H. Zhang, J. Chem. Phys. **142**, 064314 (2015).
[25]P. Sun, Z. Zhang, J. Chen, S. Liu, and D. H. Zhang, J. Chem. Phys. **149**, 064303 (2018).
[26]T. González-Lezana, P. Larrégaray, L. Bonnet, Y. Wu, and W. Bian, J. Chem. Phys. **148**, 234305 (2018).
[27]R. Ellerbrock and U. Manthe, J. Chem. Phys. **148**, 224303 (2018).
[28]A. Fernández-Ramos, J. A. Miller, S. J. Klippenstein, and D. G. Truhlar, Chem. Rev. **106**, 4518 (2006).
[29]J. Liu and W. H. Miller, J. Chem. Phys. **131**, 074113 (2009).
[30]T. J. H. Hele and S. C. Althorpe, J. Chem. Phys. **138**, 084108 (2013).
[31]D. Chandler and P. G. Wolynes, J. Chem. Phys. **74**, 4078 (1981).
[32]I. R. Craig and D. E. Manolopoulos, J. Chem. Phys. **121**, 3368 (2004).
[33]I. R. Craig and D. E. Manolopoulos, J. Chem. Phys. **122**, 084106 (2005).
[34]I. R. Craig and D. E. Manolopoulos, J. Chem. Phys. **123**, 034102 (2005).
[35]S. Habershon, D. E. Manolopoulos, T. E. Markland, and T. F. Miller III, Annu. Rev. Phys. Chem. **64**, 387 (2013).
[36]R. Collepardo-Guevara, Y. V. Suleimanov, and D. E. Manolopoulos, J. Chem. Phys. **130**, 174713 (2009).
[37]Y. V. Suleimanov, R. Collepardo-Guevara, and D. E. Manolopoulos, J. Chem. Phys. **134**, 044131 (2011).
[38]R. de Tudela, F. J. Aoiz, Y. V. Suleimanov, and D. E. Manolopoulos, J. Phys. Chem. Lett. **3**, 493 (2012).
[39]J. W. Allen, W. H. Green, Y. Li, H. Guo, and Y. V. Suleimanov, J. Chem. Phys. **138**, 221103 (2013).
[40]Y. Li, Y. V. Suleimanov, J. Li, W. H. Green, and H. Guo, J. Chem. Phys. **138**, 094307 (2013).
[41]Y. Li, Y. V. Suleimanov, W. H. Green, and H. Guo, J. Phys. Chem. A **118**, 1989 (2014).
[42]R. de Tudela, Y. V. Suleimanov, J. O. Richardson, V. Sáez Rábanos, W. H. Green, and F. J. Aoiz, J. Phys. Chem. Lett. **5**, 4219 (2014).
[43]Y. V. Suleimanov, W. J. Kong, H. Guo, and W. H. Green, J. Chem. Phys. **141**, 244103 (2014).
[44]K. M. Hickson, J.-C. Loison, H. Guo, and Y. V. Suleimanov, J. Phys. Chem. Lett. **6**, 4194 (2015).
[45]Q. Meng, J. Chen, and D. H. Zhang, J. Chem. Phys. **143**, 101102 (2015).
[46]D. J. Arseneau, D. G. Fleming, Y. Li, J. Li, Y. V. Suleimanov, and H. Guo, J. Phys. Chem. B **120**, 1641 (2016).
[47]Q. Meng, J. Chen, and D. H. Zhang, J. Chem. Phys. **144**, 154312 (2016).
[48]Q. Meng, K. M. Hickson, K. Shao, J.-C. Loison, and D. H. Zhang, Phys. Chem. Chem. Phys. **18**, 29286 (2016).
[49]Y. V. Suleimanov, F. J. Aoiz, and H. Guo, J. Phys. Chem. A **120**, 8488 (2016).
[50]J. Zuo, Y. Li, H. Guo, and D. Xie, J. Phys. Chem. A **120**, 3433 (2016).
[51]K. M. Hickson and Y. V. Suleimanov, Phys. Chem. Chem. Phys. **19**, 480 (2017).
[52]K. M. Thompson, Y. Gao, P. Marshall, H. Wang, L. Zhou, Y. Li, and H. Guo, J. Chem. Phys. **147**, 134302 (2017).
[53]J. Zuo, C. Xie, H. Guo, and D. Xie, J. Phys. Chem. Lett. **8**, 3392 (2017).
[54]K. Shao, J. Chen, Z. Zhao, and D. H. Zhang, J. Chem. Phys. **145**, 071101 (2016).
[55]Y. V. Suleimanov, J. W. Allen, and W. H. Green, Comput. Phys. Commun. **184**, 833 (2013).
[56]B. J. Braams and D. E. Manolopoulos, J. Chem. Phys. **125**, 124105 (2006).
[57]J. O. Richardson and S. C. Althorpe, J. Chem. Phys. **131**, 214106 (2009).
[58]T. J. H. Hele and Y. V. Suleimanov, J. Chem. Phys. **143**, 074107 (2015).
[59]C. H. Bennett, *Algorithms for Chemical Computations*, Volume 46 of ACS Symposium Series (American Chemical Society, 1977), pp. 63–97.
[60]D. Chandler, J. Chem. Phys. **68**, 2959 (1978).
[61]J. Kästner and W. Thiel, J. Chem. Phys. **123**, 144104 (2005).
[62]J. Kästner and W. Thiel, J. Chem. Phys. **124**, 234106 (2006).
[63]J. Kästner, J. Chem. Phys. **131**, 034109 (2009).
[64]X. Hu, W. L. Hase, and T. Pirraglia, J. Comput. Chem. **12**, 1014 (1991).
[65]D.-h. Lu, T. N. Truong, V. S. Melissas, G. C. Lynch, Y.-P. Liu, B. C. Garrett, R. Steckler, A. D. Isaacson, S. N. Rai, G. C. Hancock *et al.*, Comput. Phys. Commun. **71**, 235 (1992).
[66]F. Battin-Leclerc, I. K. Kim, R. K. Talukdar, R. W. Portmann, A. R. Ravishankara, R. Steckler, and D. Brown, J. Phys. Chem. A **103**, 3237 (1999).
[67]H. C. Andersen, J. Comput. Phys. **52**, 24 (1983).
[68]D. L. Baulch, C. T. Bowman, C. J. Cobos, R. A. Cox, T. Just, J. A. Kerr, M. J. Pilling, D. Stocker, J. Troe, W. Tsang *et al.*, J. Phys. Chem. Ref. Data **34**, 757 (2005).